BULLETIN OF THE POLISH ACADEMY OF SCIENCES
TECHNICAL SCIENCES, Vol. 69(5), 2021, Article number: e138846
DOI: 10.24425/bpasts.2021.138846

SPECIAL SECTION

Elevated-temperature tensile deformation and fracture behavior of particle-reinforced PM 8009Al matrix composite

Shuang CHEN[1], Guoqiang CHEN[1*], Pingping GAO[1, 3], Chunxuan LIU[3], Anru WU[1], Lijun DONG[1], Zhonghua HUANG[1], Chun OUYANG[1, 2, 5], and Hui ZHANG[4]**

[1] Hunan Provincial Key Laboratory of Vehicle Power and Transmission System, Hunan Institute of Engineering, Xiangtan 411104, China
[2] School of Material Science and Engineering, Jiangsu University of Science and Technology, Zhenjiang Jiangsu 21200, China
[3] Hunan Gold Sky Aluminum Industry High-tech Co., Ltd., Changsha 410205, China
[4] College of Materials Science and Engineering, Hunan University, Changsha 410082, China
[5] CETC Maritime Electronics Research Institute Co., Ltd., Ningbo Zhejiang 315000, China

Abstract. Tensile tests of 8009Al alloy reinforced with SiC and Al_2O_3 particles fabricated by powder metallurgy (PM) were conducted at temperatures of 250–350°C and strain rates of 0.001–0.1 s^{-1}. The ultimate tensile strength and yield strength of the samples decreased while the temperature and strain rate increased. The elongation slightly decreased at first and then increased with growing temperature because of the medium-temperature brittleness of the alloy matrix. When the strain rate was 0.1 s^{-1}, the elongation of the 8009Al/Al_2O_3 composites always decreased with an increase in temperature because of the poorly coordinated deformation and weak bonding between the matrix and Al_2O_3 particles at such a high strain rate. The work-hardening rates of the composites sharply increased to maxima and then decreased rapidly as the strain increased. Meanwhile, the 8009Al/SiC_p composites displayed superior UTS, YS, elongation, and work-hardening rates than those of the 8009Al/Al_2O_3 composites under the same conditions. Compared to 8009Al alloys reinforced with spherical Al_2O_3 particle, 8009Al alloys reinforced with irregular SiC particles exhibited a better strengthening effect. The fracture mechanism of the 8009Al/SiC_p composites was mainly ductile, while that of the 8009Al/Al_2O_3 composites was primarily debonding at the matrix–particle interfaces in a brittle mode.

Key words: aluminum matrix composite; 8009Al alloy; elevated-temperature tensile property; interface; fracture behavior.

1. INTRODUCTION

Al-matrix composites reinforced with hard ceramic particles are widely used in the aerospace aera, defense department, and automotive industries because of their excellent performance including high strength, high stiffness, good corrosion resistance, light weight, and thermal stability [1–3]. Among these, Al-Fe-V-Si alloys and composites reinforced with ceramic particles are very broadly utilised at evaluated temperatures due to large volumes of very fine dispersed $Al_{12}(Fe,V)_3Si$ particles. Thus, they are expected to be good heat-resistant substitutes for Ti alloys at 300–400 °C [4, 5]. Nevertheless, reinforcement particles, such as SiC, TiC, and Al_2O_3, and/or high-volume fractions of very fine $Al_{12}(Fe,V)_3Si$ induce poor formability and hot workability of Al-Fe-V-Si alloys and composites, thus their usage is limited.

Most studies on deformation characteristics have focused on Al-Fe-V-Si alloys. The hot-working characteristics of rapidly solidified Al-8.5Fe-l.3V-l.7Si (8009) and Al-12.4Fe-l.2V-2.3Si (FVS1212) were investigated by isothermal hot torsion testing at temperatures of 300–600 °C and strain rates of 0.1–4.0 s^{-1} [6]. The deformation characteristics of the rapidly solidified dispersion-strengthened 8009Al alloy processed by planar flow casting were studied by tensile testing at the temperatures of 25–420 °C and compression and hardness testing at 25 °C [7]. In addition, the tensile deformation behavior of the spray-deposited 8009Al alloy was investigated by uniaxial tension testing at temperatures of 250–450 °C and strain rates of 0.001–0.1 s^{-1} [4]. Furthermore, the high-temperature plastic deformation behavior of spray-deposited 8009Al alloy was examined by compression testing at strain rates of 2.77×10^{-4}–2.77×10^{-2} s^{-1} and temperatures of 350–550 °C [8]. Al-Fe-V-Si Al alloys were prepared by the method of electron beam melting, which exhibits grain microstructure and good mechanical properties [9]. SiCp/Al-Fe-V-Si produced by spray-deposited displays better-elevated temperature mechanical properties, tensile fracture behavior, and thermal stability [10, 11].

The content of reinforcement can be accurately controlled in any proportion via powder metallurgy (PM), and the reinforcement particles can distribute uniformly in the matrix, leading to stable performance and high production efficiency in the prepared material. The authors [12, 13] previously investigated the characteristics and mechanisms of hot deformation and particle-reinforced mechanism of 8009Al matrix

e-mail: *chengq1979@163.com, **oyc1014@just.edu.cn

Manuscript submitted 2021-04-19, revised 2021-07-02, initially accepted for publication 2021-07-28, published in October 2021

© 2021 The Author(s). This is an open access article under the CC BY license (http://creativecommons.org/licenses/by/4.0/).

composite 8009Al/SiC_p and 8009Al/Al_2O_3 at temperatures of 400–550 °C and strain rates of 0.001–1 s^{-1} by hot compression testing. However, few studies on the tensile and fracture behaviors of PM-processed ceramic particle-reinforced Al-Fe-V-Si alloy matrix composites have been reported. In the present work, uniaxial tension tests were performed on 8009Al/SiC_p and 8009Al/Al_2O_3 composites at temperatures of 250–350 °C and strain rates of 0.001–0.1 s^{-1}. The elevated-temperature tensile deformation of 8009Al/SiC_p and 8009Al/Al_2O_3 composites was investigated. Similarly, the effects of the tensile temperature and strain rate on the strength, elongation, and work-hardening rate were described. In addition, the fracture mechanisms of 8009Al/SiC_p and 8009Al/Al_2O_3 composites were investigated at different temperatures and strain rates. The present work is significant for understanding the hot tensile and fracture behaviors of PM-processed ceramic particle-reinforced Al matrix composites.

2. MATERIAL AND METHODS

The 8009Al alloy matrix samples with a chemical composition of 8.42 wt.% Fe, 1.29 wt.% V, 1.93 wt.% Si, and the balance of Al were prepared by rapid solidification. Irregular SiC particles and spherical Al_2O_3 particles with the same volume fraction of 15% were used separately as reinforcements; their average diameters were approximately 10 μm and 5 μm, respectively. First, the composites were fabricated by PM and extrusion. The homogeneous mixed reinforcements (SiC or Al_2O_3) and 8009Al alloy matrix powders after canning, vacuum degassing, and densification were extruded into 53-mm diameter bars by using an 1800 T extrusion machine when the temperature is 460 °C and the extrusion speed is 0.5 mm/s. The bars were then machined into 20-mm thick plates by linear cutting along the extrusion direction. After that, the plates were heated at 500 °C for 2 h and subsequently hot-rolled into the final 1.4-mm-thick sheets along the extrusion direction with approximately 10% thickness reduction in every pass. The densities of 8009Al/SiC_p and 8009Al/Al_2O_3 composites were 2.822 g/cm^3 and 2.876 g/cm^3, respectively.

The tension specimens with a gauge length of 10 mm, a width of 3 mm, and a thickness of 1.40 mm were cut parallel to the rolling direction. The tension tests were conducted using a computer-controlled Instron-3382 machine at temperatures from 250 °C to 350 °C and strain rates from 0.001 s^{-1} to 0.1 s^{-1}, respectively. The samples were heated to the predetermined tensile testing temperatures at a heating rate of 5 °C/s and held at these temperatures for 10 min to ensure temperature homogeneity throughout each sample before tensile testing. The phase constituents and microstructures of rolled sheets were characterized by X-ray diffraction (XRD) patterns with a Siemens D5000 diffractometer system and optical microscopy (OM; MM-6). Fracture surfaces were examined by scanning electron microscopy (SEM; FEI QUANTA 200).

3. RESULTS AND DISCUSSION

3.1. Microstructures of the as-rolled sheets

Figure 1 shows the microstructures and X-ray diffraction (XRD) patterns of the as-rolled 8009Al/SiC_p and 8009Al/Al_2O_3 composite sheets. The optical microscopy (OM) image in Fig. 1a indicates that the irregularly shaped SiC particles with an average diameter of 10 μm are uniformly distributed in the 8009Al alloy matrix. The spherical Al_2O_3 particles have diameters of 1–50 μm, with an average size of about 5 μm, and are homogeneously distributed in the 8009Al alloy matrix (Fig. 1b). The XRD pattern in Fig. 1c reveals that the 8009Al/SiC_p composites contain α-Al, β-SiC, and $Al_{12}(Fe,V)_3Si$ phases and the 8009Al/Al_2O_3 composites consist of α-Al, Al_2O_3, and $Al_{12}(Fe,V)_3Si$ phases.

3.2. Tensile behavior

Figure 2 shows a series of tensile engineering stress–engineering strain curves of the studied 8009Al/SiC_p composites at different temperatures and strain rates. The curves clearly exhibit similar tendencies under different deformation conditions, in which the stress increases linearly and sharply with increasing strain at first. It reaches a peak after uniform plastic deformation and subsequently exhibits flow softening until the material eventually breaks except for a strain rate of 0.001 s^{-1}. In addition, the strain range corresponding to the softening stage of the 8009Al/SiC_p composites increases gradually with an increasing strain rate and temperature and reaches a maximum at a strain rate of 0.1 s^{-1} and temperature of 350 °C, as shown in Fig. 2c. The tensile samples deformed to fracture exhibit almost

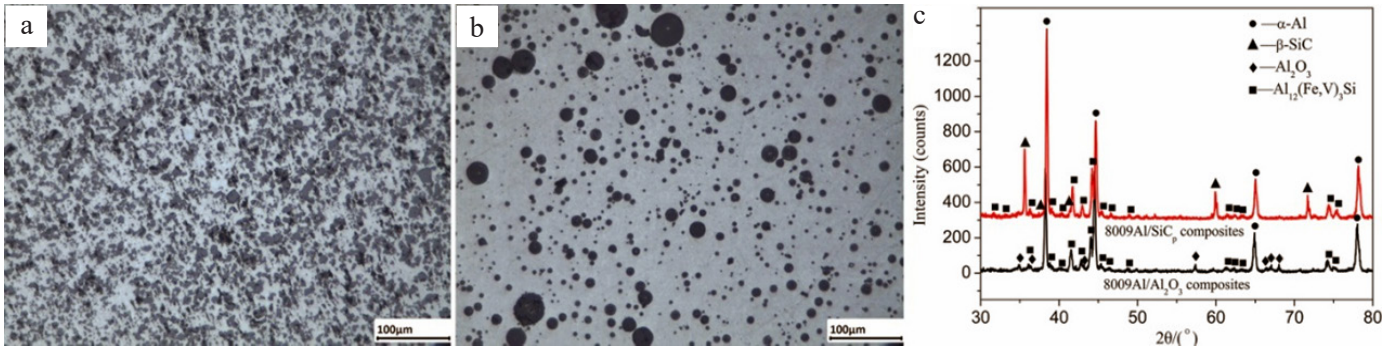

Fig. 1. Microstructure of as-rolled 8009Al matrix composites; (a) OM image of as-rolled 8009Al/SiC_p composites; (b) OM image of as-rolled 8009Al/Al_2O_3 composites and (c) XRD pattern

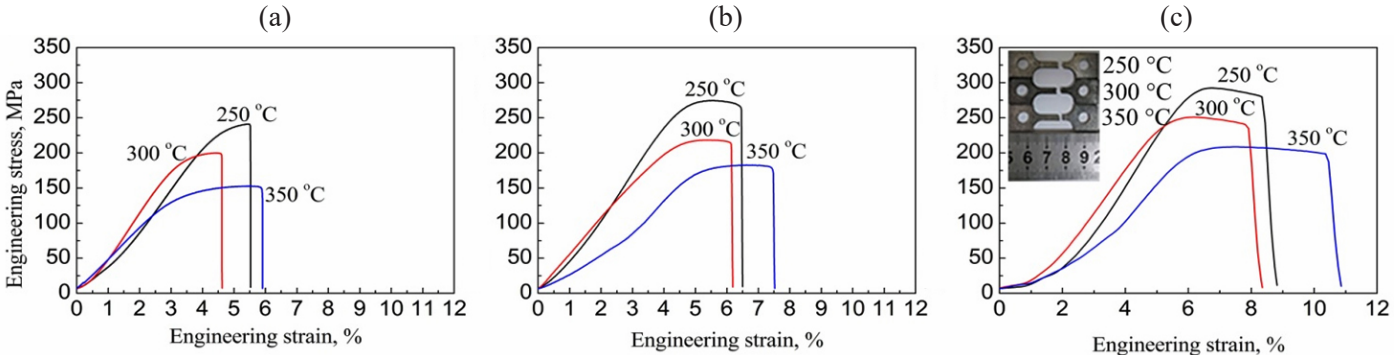

Fig. 2. The engineering stress–engineering strain curves of the studied 8009Al/SiC_p composites under different high temperature tensile deformation conditions: (a) 0.001 s^{-1}; (b) 0.01 s^{-1}; (c) 0.1 s^{-1}

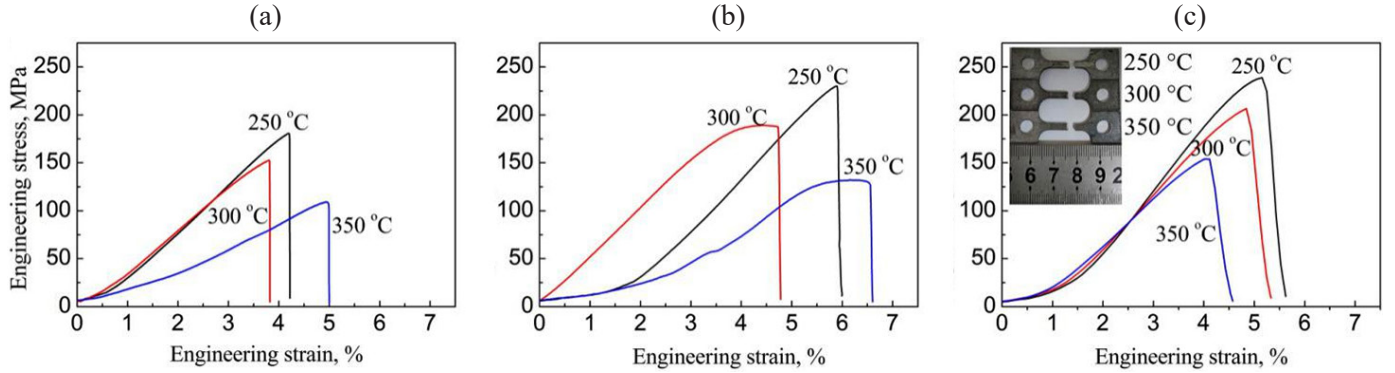

Fig. 3. The engineering stress–engineering strain curves of the studied 8009Al/Al_2O_3 composites under different high temperature tensile deformation conditions: (a) 0.001 s^{-1}; (b) 0.01 s^{-1}; (c) 0.1 s^{-1}

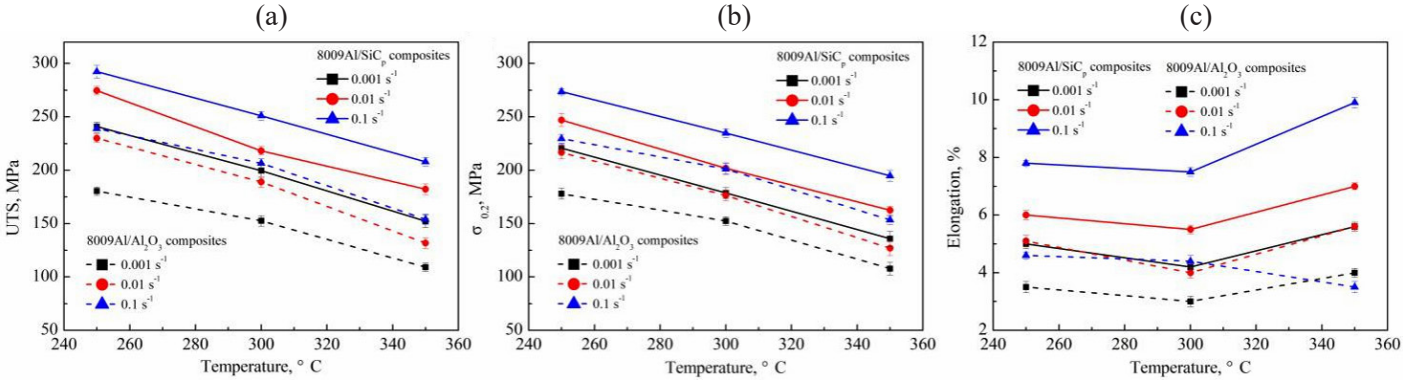

Fig. 4. Temperature dependence of ultimate tensile strength (UTS) (a); yield strength (YS) (b) and total elongation to failure (c) of 8009Al/SiC_p and 8009Al/Al_2O_3 composites at various strain rate

no necking at a strain rate of 0.1 s^{-1} in the tensile temperature range of 250–350 °C in the sample photographs in Fig. 2c. Therefore, the flow stress decrease is considered irrelevant to necking, which may be related to dynamic recovery [14–16].

The engineering stress–engineering strain curves of the 8009Al/Al_2O_3 composites at different temperatures and strain rates are presented in Fig. 3. Obviously, the stress-strain curves of the 8009Al/Al_2O_3 composites are significantly different from those of 8009Al/SiC_p composites. In Figure 3, the flow stresses of the 8009Al/Al_2O_3 composites grow with an increasing strain. Subsequently, the tensile specimen fracture when the stress reaches the ultimate tensile strength (UTS), and almost no dynamic softening exists under any of the tensile conditions. This characteristic is attributed to the shapes, types, and wettability of the reinforcing particles [10, 17–19].

Figure 4 shows the effects of the temperature and strain rate on the UTS, yield strength (YS), and total elongation to failure of the 8009Al/SiC_p and 8009Al/Al_2O_3 composites. The relationships among the UTS, YS, temperatures, and strain rates of the 8009Al/SiC_p and 8009Al/Al_2O_3 composites are similar, as shown in Figs. 4a and 4b. The UTS and YS of both kinds of composites decrease with an increasing temperature

and decreasing strain rate, which is similar to the case for the previously investigated spray-deposited SiC_p/Al-Fe-V-Si composites [10]. This finding can be attributed to the activation of more dislocation slip systems and dynamic recovery at higher temperatures, as well as the higher thermal energy at higher temperatures and increased time provided by lower strain rates, which together help the dislocations overcome obstacles, resulting in reduced flow stress [12, 20–22]. In addition, the 8009Al/SiC_p composites display superior UTS, and YS compared with the 8009Al/Al_2O_3 composites under the same tensile deformation conditions, as shown in Figs. 1a and 1b. This superiority may be associated with the difference between the degrees of binding of the two kinds of reinforcing particles with the matrices, causing them to fracture via different mechanisms.

Table 1 gives the specific data of UTS and YS of 8009Al/SiC_p and 8009Al/Al_2O_3 composites at a strain rate of 0.1 s^{-1}. The results show that compared with the 8009Al/Al_2O_3 composites the UTS of 8009Al/SiC_p composites at deformation temperatures of 250 °C, 300 °C, and 350 °C are increased by 53.4%, 44.3%, and 53.9%, respectively, and YS are increased by 44%, 33.6%, and 41.3%, respectively. In summary, the strengthening effect of 8009Al/SiC_p composites is better than that of 8009Al/Al_2O_3 composites.

TABLE 1
Strength data of particle reinforced 8009Al matrix composites at strain rate of 0.1 s^{-1}

Material Tensile temperature (°C)	8009Al/SiC_p composites		8009Al/Al_2O_3 composites	
	UTS (MPa)	YS (MPa)	UTS (MPa)	YS (MPa)
250	292.4 ± 6	273.6 ± 3	239.0 ± 4	229.6 ± 4
300	250.9 ± 4	234.8 ± 4	206.6 ± 4	201.2 ± 5
350	207.9 ± 4	194.7 ± 5	154.0 ± 5	153.4 ± 4

In Figure 4c, the elongation of the 8009Al/SiC_p composites slightly decreases at first and then increases as the tensile temperature increases from 250 °C to 350 °C. The lowest elongation appears at 300 °C for all the strain rates. This behavior is different from those reported previously for a spray-deposited FVS0812 heat-resistant aluminum alloy sheet [4] and spray-deposited SiC_p/Al-Fe-V-Si composite [10], where the elongation increased with the increasing tensile temperature. This difference may be related to the medium-temperature embrittlement of Al-Fe-V-Si alloy matrices from rapid solidification. The medium-temperature embrittlement of rapidly solidified heat-resistant Al alloys often occurs at temperatures of 100–300 °C [23, 24]. New dislocation sources are constantly activated with the increasing temperature and external force. A higher temperature also provides thermal energy to facilitate simultaneous dislocation slipping and climbing. With the increasing strain, dynamic recovery becomes increasingly dominant, causing a decrease in the number of open dislocation sources, most of which are located at special interfaces, such as sub-grain, grain, or phase boundaries.

In the present composites, because of the strong effects of massive SiC_p or Al_2O_3 particles, easy dislocation migration paths are interrupted during deformation at a particular temperature. Therefore, the localization of microscopic deformation could be the result. Cracks first emerge and expand rapidly in these areas, and regionally concentrated damage is produced, causing material fracture by the early instability of the macroscopic plastic deformation. The elongation of the 8009Al/SiC_p composites increases with an increasing strain rate at all temperatures from 250 °C to 350 °C. The greatest elongation of 9.9% for the 8009Al/SiC_p composites occurs at 350 °C and 0.1 s^{-1}. Furthermore, the elongation of the 8009Al/Al_2O_3 composites varies similarly to that of the 8009Al/SiC_p composites, except at a strain rate of 0.1 s^{-1}, where the elongation of the 8009Al/Al_2O_3 composites decreases as the tensile temperature increases from 250 °C to 350 °C. This behavior can be attributed to the easier plastic deformation of the matrix alloy at high temperatures, which induces poorly coordinated deformation between the matrix and Al_2O_3 enhanced particle interface at high strain rates. Meanwhile, the bonding between the Al_2O_3 particles and matrix alloy is relatively weak. Debonding, crack formation, instability, and fracturing tend to occur during tensile processes when the deformation conditions are unfavorable, leading to the rapid reduction of the elongation of the 8009Al/Al_2O_3 composites at 350 °C and 0.1 s^{-1}. Meanwhile, the elongation of the 8009Al/SiC_p composites is greater than that of the 8009Al/Al_2O_3 composites in almost all the given deformation conditions, which is a result of their different fracture mechanisms.

3.3. Work-hardening behavior

Work-hardening behavior of the composites can be described by the work-hardening rate ($\theta = \partial\sigma/\partial\varepsilon$, where σ is the true stress and ε is the true strain) [25]. Figure 5 shows the work-hardening rate versus the true strain under different deformation

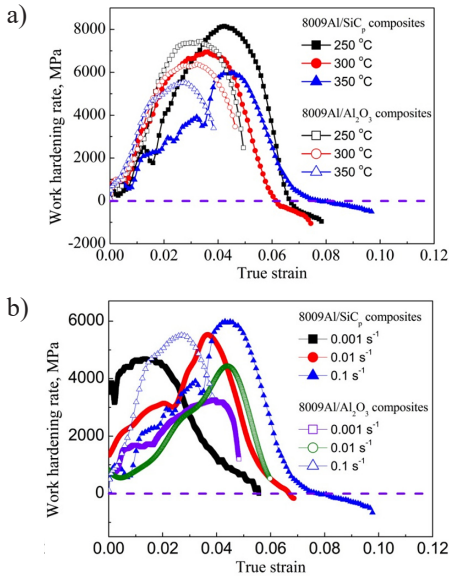

Fig. 5. Work-hardening rate–true strain curves of the 8009Al matrix composites: (a) at the strain rate of 0.1 s^{-1} and (b) at the temperature of 350 °C

conditions of the 8009Al matrix composites. The work-hardening rates of the composites show similar trends and can be divided into two stages. The work-hardening rate sharply increases as the true strain increases and reaches a maximum value in stage I. This behavior may arise from the high dislocation density generated with increasing strain, the high-volume fraction of $Al_{12}(Fe,V)_3Si$-phase dispersoids, and SiC_p/Al_2O_3 reinforcing particles, which can strongly hinder the dislocation motion. The high-density dislocations experience pinning become tangled, respond, and reorganize, which increases the work-hardening rate [11, 13]. In stage II, as the strain increases, the work-hardening rate decreases rapidly. This characteristic can be attributed to the dynamic recovery, the decrease in the dislocation density, the cracking of the reinforced particles, the debonding of the reinforced particles from the Al matrix interface, and so on [10, 26].

Figure 5a shows the variation of the work-hardening rate with strain for the 8009Al matrix composites at a strain rate of 0.1 s^{-1}. The temperature sharply influences the work-hardening rate. The work-hardening rate of the $8009Al/SiC_p$ or $8009Al/Al_2O_3$ composites decreases with an increasing temperature, and the work-softening rate of the $8009Al/SiC_p$ composites appears to be negative with an increasing strain, which corresponds to a decrease in tensile stress. Figure 5b further illustrates the work-hardening rates for the 8009Al matrix composites at different strain rates and demonstrates that a higher work-hardening rate occurs at a higher strain rate. Moreover, the work-hardening rates of the $8009Al/SiC_p$ composites are higher than those of the $8009Al/Al_2O_3$ composites under the same conditions in Fig. 5.

3.4. Fracture behavior

Figure 6 shows the fracture surfaces of the $8009Al/SiC_p$ composites tested at the temperatures of 250–350 °C and strain rates of 0.001–0.1 s^{-1}. The dimples are distributed throughout the 8009Al alloy matrix fracture surface, which indicates that ductile fracturing according to the micro void growth and coalescence is the primary fracture mechanism of the studied $8009Al/SiC_p$ composites [27–29]. However, the dimples are very fine and shallow under any given experimental deformation conditions

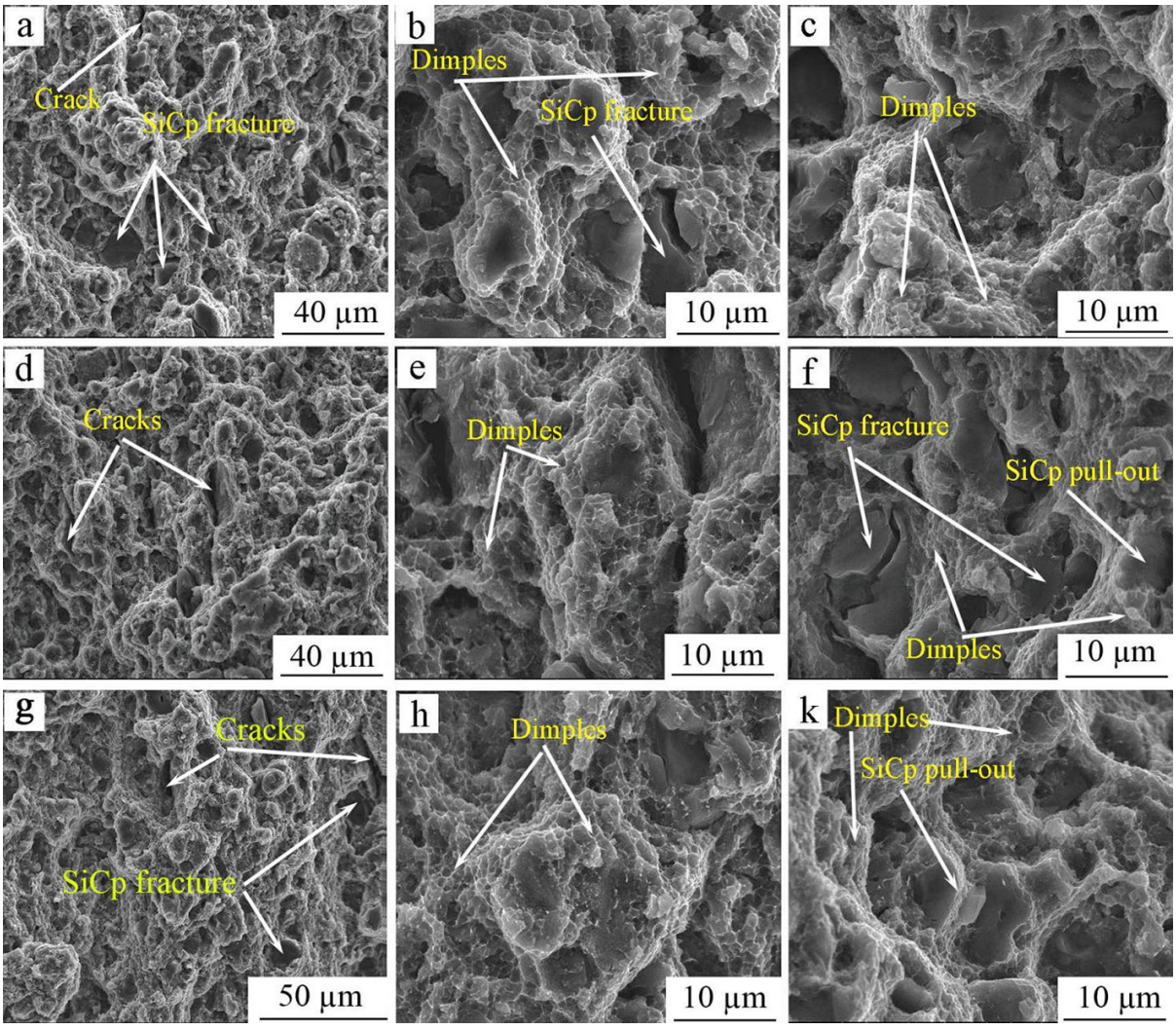

Fig. 6. SEM fractography of the $8009Al/SiC_p$ composites obtained under different tensile deformation conditions: a) 250 °C, 0.001 s^{-1}; b) 250 °C, 0.001 s^{-1}; c) 250 °C, 0.1 s^{-1}; d) 300 °C, 0.001 s^{-1}; e) 300 °C, 0.001 s^{-1}; f) 300 °C, 0.1 s^{-1}; g) 350 °C, 0.001 s^{-1}; h) 350 °C, 0.001 s^{-1}; k) 350 °C, 0.1 s^{-1}

in Figs. 6a–k, indicating that small plastic deformations occur in the 8009Al/SiC_p composites. This feature can be attributed to the high volume fraction of very fine $Al_{12}(Fe, V)_3Si$-phase dispersoids distributed mainly along the smaller grain boundary of the 8009Al alloy matrix, which effectively prevents matrix grain growth and dynamic recrystallization behavior [4, 13]. Along with the increase in tensile stress, the voids nucleate at the interfaces between the matrix and $Al_{12}(Fe, V)_3Si$-phase dispersoids, then undergo growth and coalescence via ductile shearing, eventually leading to dimpled fracture [4, 5]. In addie tion, the dimples in the matrix become much larger and deeper with an increasing strain rate in Fig. 6, which indicates that the plastic deformation of the matrix increases with an increasing strain rate. The dimples in the matrix at 250 °C and 300 °C have nearly the same size and depth, as shown in Figs. 6a–6f, and the dimples are larger and deeper at 350 °C in Figs. 6g–6k. The variation in fracture strain is the same as that of the studied 8009Al/SiC_p composites, which can be attributed to the higher thermal activation energy at 350 °C and the effect of the previously mentioned medium-temperature embrittlement at 200–300 °C [24, 30].

Moreover, the enhancement of the ceramic particles in the composites is related to the bonding properties of the interface between the ceramic particles and alloy matrix and the uniform distribution of the ceramic particles in the alloy matrix. In Figure 6, most of the SiC particles break to form new smooth surfaces and a few characteristics of SiC particle pull-out can be observed in the fracture surfaces of the 8009Al/SiC_p composites, which show a good interface formation between the SiC particles and alloy matrix [11]. Based on the authors' previous research [12, 13], it is believed that there are two kinds of an interface between Al matrix composites prepared by PM and extrusion, i.e., slight reaction interface and clean interface, which are the same as those reported by others [31–33]. Meanwhile, the interaction between the added SiC particles and Al matrix is thought to be the main reason for good interface formation by He *et al*. [10] and Hao *et al*. [11]. The chemical reaction products, i.e., the Si and Al_4C_3 phases distribute at the SiC_p/Al matrix interface, and the resultant Si can diffuse into an Al matrix to improve the wettability of the SiC_p/Al matrix interface; accordingly, the bonding between the SiC particles and alloy matrix is strong [10, 34, 35]. Meanwhile, the new smooth surfaces also demonstrate that the SiC particles experience tremendous loads transferred from the Al matrix, because of the mismatch between the elastic constants, which can enhance the load transfer of the studied PM 8009Al/SiC_p composites. The number of fractured SiC particles decreases (a 98%; d 96%; f 92%; k 90%) and the quantity of pulled out SiC particles increases with an increasing temperature and strain rate, as shown in Fig. 6. This characteristic can be attributed to the weakening bonding between the SiC particles and alloy matrix with an increasing temperature. In summary, the fracture mechanism of the studied 8009Al/SiC_p composites is mainly ductile fracturing according to the micro void growth and coalescence, accompanied by a very small amount of brittle fracturing. Furthermore, SiC particle cracking and/or interfacial debonding between the SiC particles and matrix not only undermine the local continuity of the materials but also decrease the cross-sectional areas of the 8009Al/SiC_p composite specimens under tension significantly reduce the flow stress of the materials and induce premature fracturing and failure [36, 37].

The fracture surfaces of the 8009Al/Al_2O_3 composites under different conditions after high-temperature tensile testing are shown in Fig. 7 and exhibit characteristics significantly differ-

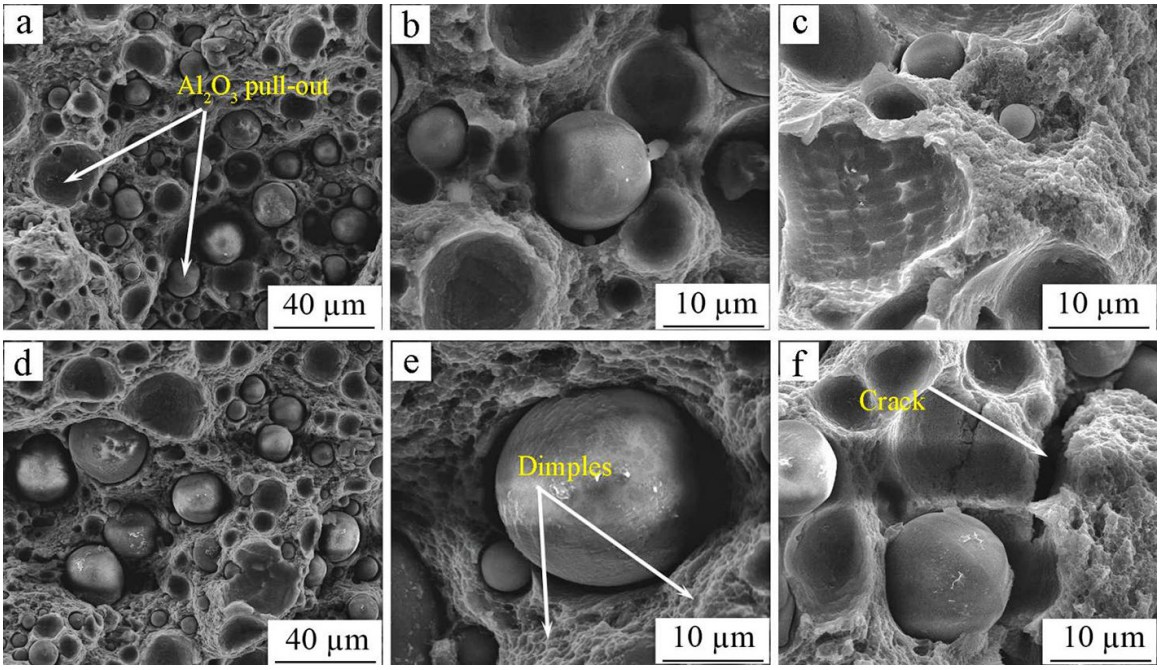

Fig. 7. SEM fractography of the 8009Al/Al_2O_3 composites obtained under different tensile deformation conditions: a) 250 °C, 0.001 s^{-1}; b) 250 °C, 0.001 s^{-1}; c) 250 °C, 0.1 s^{-1}; d) 350 °C, 0.001 s^{-1}; e) 350 °C, 0.001 s^{-1}; f) 350 °C, 0.1 s^{-1}

ent from those of 8009Al/SiC_p composites. As shown in Fig. 7, nearly all of the Al_2O_3 particles are pulled out, which indicates a poor combined surface bonding between the Al_2O_3 particles and Al matrix, probably because the unreacted appropriate product appears at the Al_2O_3/Al matrix interface and does not improve its wettability [38]. Meanwhile, spherical Al_2O_3 particles have lower wettability on an Al matrix. In Fig. 7, some relatively large cavities are present, dimples are not evident under most deformation conditions, and small dimples can be observed only at 350 °C and 0.001 s^{-1} in Fig. 7e. Thus, plastic deformation of the 8009Al/Al_2O_3 composites is not highly developed and brittle fracturing is the primary fracture mode [39–41]. Therefore, the wettability of irregular SiC particles with an 8009Al alloy matrix is different from that of spherical Al_2O_3 particles, causing differences in the actual fracture mechanisms of the two kinds of particle-reinforced PM 8009Al matrix composites [10, 11, 19].

4. CONCLUSIONS

The tensile deformation and fracture behavior of particle-reinforced PM 8009Al matrix composites were studied at temperatures of 250–350 °C and strain rates of 0.001–0.1 s^{-1}. The results can be summarized as follows:

- The UTS and YS of particle-reinforced PM 8009Al matrix composites decreased with an increasing temperature and decreasing strain rate. The elongation of the studied composites slightly decreased at first and then increased with an increasing tensile temperature except when the strain rate was 0.1 s^{-1}, in which case the elongation of the 8009Al/Al_2O_3 composites always decreased with an increasing tensile temperature because of the strain incompatibility and weak bonding between the matrix and Al_2O_3 particles at high strain rates. Meanwhile, the 8009Al/SiC_p composites displayed superior UTS, YS, and elongation compared with the 8009Al/Al_2O_3 composites under the same tensile deformation conditions. The irregular SiC particles exhibited better strengthening effects than the spheroidal Al_2O_3 particles in the studied 8009Al matrix composites.
- The work-hardening rate of particle-reinforced PM 8009Al matrix composites sharply increased to a maximum and then decreased rapidly as the true strain increased. Higher work-hardening rates could be obtained at higher strain rates and lower temperatures.
- The fracture modes of particle-reinforced PM 8009Al matrix composites depended on the reinforcement type. The fracture mechanism of the 8009Al alloys reinforced with SiC particles was mainly ductile fracturing according to the micro void growth and coalescence with a very small amount of brittle fracturing. The cracking of the SiC particles gradually decreased but bonding at the Al matrix-particle interfaces increased with an increasing temperature and strain rate. Debonding at the matrix-particle interfaces was the dominant cracking mode and brittle fracturing was the primary fracture mechanism for the 8009Al alloys reinforced with Al_2O_3 particles.

ACKNOWLEDGEMENTS

The authors acknowledge the financial support from Project (2020JJ6015, 2019JJ60035) supported by the Natural Science Foundation of Hunan Province China. Projects(18A350, 19A118) supported by Scientific Research Fund of Hunan Provincial Education Department, China. This work was also supported by the Natural Science Foundation of Jiangsu Province, China (Grant No. BK20190973) and the Preferential funding of Zhejiang Post-Doctoral Research Projects (Grant No. ZJ2020085).

REFERENCES

[1] P.-h. Lü, X.F. Wang, C.G. Dong, C.Q. Peng, and R.C. Wang, "Preparation and characterization of different surface modified SiCp reinforced Al-matrix composites," *J. Cent. South Univ.*, vol. 27, no. 9, pp. 2567–2577, 2020, doi: 10.1007/s11771-020-4482-z.

[2] C. Emmy Prema, S. Suresh, G. Ramanan, and M. Sivaraj, "Characterization, corrosion and failure strength analysis of Al7075 influenced with B_4C and Nano-Al_2O_3 composite using online acoustic emission," *Mater. Res. Express*, vol. 7, no. 1, pp. 016524, 2020, doi: 10.1088/2053-1591/ab6257.

[3] S.V. Nair, J.K. Tien, and R.C. Bates, "SiC-reinforced aluminium metal matrix composites International Metals Reviews," *Int. Met. Rev.*, vol. 30, no. 1, pp. 275–290, 1985, doi: 10.1179/imtr.1985.30.1.275.

[4] Q. Yan, D. Fu, X. Deng, H. Zhang, and Z. Chen, "Tensile deformation behavior of spray-deposited FVS0812 heat-resistant aluminum alloy sheet at elevated temperatures," *Mater. Charact.*, vol. 58, no. 6, pp. 575–579, 2007, doi: 10.1016/j.matchar.2006.06.024.

[5] Z.H. Chen, Y.Q. He, H.G. Yan, Z.G. Chen, X.J. Yin, and G. Chen, "Ambient temperature mechanical properties of Al-8.5Fe-1.3V-1.7Si/SiC_P composite," *Mater. Sci. Eng. A*, vol. A460–61, no. Jul, pp. p.180–185, 2007, doi: 10.1016/j.msea.2007.02.105.

[6] D. Shimansky and H.J. McQueen, "Hot Working Of Heat Resistant Rapidly Solidified AI-Fe-V-Si Alloy," *High Temp. Mat.*, vol. 18, no. 4, pp. 241–252, 1999, doi: 10.1515/HTMP.1999.18.4.241.

[7] S. Hariprasad, S. Sastry, and K.L. Jerina, "Deformation behavior of a rapidly solidified fine grained Al-8.5%Fe-1.2%V-1.7%Si alloy," *Acta. Mater.*, vol. 44, no. 1, pp. 383–389, 1995, doi: 10.1016/1359-6454(95)00160-1.

[8] Y.D. Xiao, W. Wang, and L.I. Wen-Xian, "High temperature deformation behavior and mechanism of spray deposited Al-Fe-V-Si alloy," *Trans. Nonferrous Met. Soc. China*, vol. 17, no. 006, pp. 1175–1180, 2007, doi: 10.1016/S1003-6326(07)60245-3.

[9] S. Sun, L. Zheng, P. Hui, and Z. Hu, "Microstructure and mechanical properties of Al-Fe-V-Si aluminum alloy produced by electron beam melting," *Mater. Sci. Eng. A*, vol. 659, no. 6, pp. 207–214, 2016, doi: 10.1016/j.msea.2016.02.053.

[10] Y. He, H. Tu, B. Qiao, L. Feng, J. Yang, and Y. Sun, "Tensile fracture behavior of spray-deposited SiC_P/Al–Fe–V–Si composite sheet," *Adv. Compos. Mater.*, vol. 22, no. 4, pp. 227–237, 2011, doi: 10.1080/09243046.2013.796626.

[11] L. Hao, Y.Q. He, N. Wang, Z.H. Chen, Z.G. Chen, H.G. Yan, and Z.K. Xu, "The Thermal Stability and Elevated Temperature Mechanical Properties of Spray-Deposited SiC_P/Al–11.7Fe–1.3V–1.7Si Composite," *Adv. Compos. Mater.*, vol. 18, no. 4, pp. 351–364, 2009, doi: 10.1163/156855109X434766.

[12] S. Chen, D. Fu, H. Luo, Y. Wang, J. Teng, and H. Zhang, "Hot workability of PM 8009Al/Al_2O_3 particle-reinforced composite characterized using processing maps," *Vacuum*, vol. 149, pp. 297–305, 2018, doi: 10.1016/j.vacuum.2018.01.001.

[13] C. Shuang, T. Jie, H. Luo, W. Yu, and Z. Hui, "Hot deformation characteristics and mechanism of PM 8009Al/SiC particle reinforced composites," *Mater. Sci. Eng. A*, vol. 697, pp. 194–202, 2017, doi: 10.1016/j.msea.2017.05.016.

[14] M.H. Guo, J. Y. Liu, C.C. Jia, Q.J. Jia, and S.J. Guo, "Microstructure and properties of electronic packaging shell with high silicon carbide aluminum-base composites by semi-solid thixoforming," *J. Cent. South Univ.*, vol. 21, no. 11, pp. 4053–4058, 2014, doi: 10.1007/s11771-014-2396-3.

[15] H.S. Chen, W.X. Wang, H.H. Nie, J. Zhou, Y.L. Li, R.F. Liu, Y.Y. Zhang, and P. Zhang, "Microstructure evolution and mechanical properties of B_4C/6061Al neutron absorber composite sheets fabricated by powder metallurgy," *J Alloys Compd.*, vol. 730, pp. 342–351, 2018, doi: 10.1016/j.jallcom.2017.09.312.

[16] H.S. Chen, W.X. Wang, Y.L. Li, P. Zhang, H.H. Nie, and Q.C. Wu, "The design, microstructure and tensile properties of B4C particulate reinforced 6061Al neutron absorber composites," *J. Alloy. Compd.*, vol. 632, pp. 23–29, 2015, doi: 10.1016/j.jallcom.2015.01.048.

[17] H. Sun, X. Li, P. Zhang, and W. Fang, "The microstructure and tensile properties of the Ti_2AlC reinforced TiAl composites fabricated by powder metallurgy," *Mater. Sci. Eng. A*, vol. 611, pp. 257–262, 2014, doi: 10.1016/j.msea.2014.06.009.

[18] W. Zhang, D. Chai, G. Ran, and J.E. Zhou, "Study on microstructure and tensile properties of in situ fiber reinforced aluminum matrix composites," *Mater. Sci. Eng. A*, vol. 476, no. 1/2, pp. 157–161, 2008, doi: 10.1016/j.msea.2007.05.018.

[19] S. Ghanaraja, K.L.V. Kumar, K.S. Ravikumar, and B.M. Madhusudan, "Mechanical Properties of Al_2O_3 Reinforced Cast and Hot Extruded Al based Metal Matrix Composites," *Mater. Today: Proc.*, vol. 4, no. 2, Part A, pp. 2771–2776, 2017, doi: 10.1016/j.matpr.2017.02.155.

[20] M. Sharififar and S. Mousavi, "Tensile deformation and fracture behavior of CuZn5 brass alloy at high temperature," *Mater. Sci. Eng. A*, vol. 594, no. 1, pp. 118–124, 2014, doi: 10.1016/j.msea.2013.11.051.

[21] D. Hull and D. J. Bacon, *Introduction to Dislocations*,4th Ed., 2001, Oxford.

[22] H. Luo, J. Teng, S. Chen, Y. Wang, and H. Zhang, "Flow stress and processing map of a PM 8009Al/SiC particle reinforced composite during hot compression," *J. Mater. Eng. Perform.*, vol. 26, no. 10, pp. 4789–4796, 2017, doi: 10.1007/s11665-017-2963-5.

[23] E. Bouchaud, L. Kubin, and H. Octor, "Ductility and dynamic strain ageing in rapidly solidified aluminium alloys. Metall Trans 22A:1021–1028," *Metall. Trans. A*, vol. 22, no. 5, pp. 1021–1028, 1991, doi: 10.1007/BF02661095.

[24] D.M. Li and A. Bakker, "Temperature and strain rate dependence of the portevin-le chatelier effect in a rapidly solidified Al alloy," *Metall. Mater. Trans.*, vol. 26, no. 11, pp. 2873–2879, 1995, doi: 10.1007/BF02669645.

[25] L. Yuan, W. Shi, Z. Zheng, and D. Shan, "Effect of the aspect ratio of whisker on work-hardening rate of as forged 2024Al/$Al_{18}B_4O_{33}$w composite," *Mater. Charact.*, vol. 104, pp. 73–80, 2015, doi: 10.1016/j.matchar.2015.04.006.

[26] W.J. Li, K.K. Deng, X. Zhang, C.J. Wang, J.W. Kang, K.B. Nie, and W. Liang, "Microstructures, tensile properties and work-hardening behavior of SiCp/Mg-Zn-Ca composites," *J. Alloy. Compd.*, vol. 695, pp. 2215–2223, 2016, doi: 10.1016/j.jallcom.2016.11.070.

[27] T.S. Srivatsan, M. Al-Hajri, C. Smith, and M. Petraroli, "The tensile response and fracture behavior of 2009 aluminum alloy metal matrix composite," *Mater. Sci. Eng. A*, vol. 346, no. 1–2, pp. 91–100, 2003, doi: 10.1016/S0921-5093(02)00481-1.

[28] M. Vedani, F. D'Errico, and E. Gariboldi, "Mechanical and fracture behaviour of aluminium-based discontinuously reinforced composites at hot working temperatures," *Compos. Sci. Technol*, vol. 66, no. 2, pp. 343–349, 2006, doi: 10.1016/j.compscitech.2005.04.045.

[29] J.Y. Bai, C.L. Fan, S.B. Lin, C.L. Yang, and B.L. Dong, "Mechanical Properties and Fracture Behaviors of GTA-Additive Manufactured 2219-Al After an Especial Heat Treatment," *J. Mater. Eng. Perform.*, vol. 26, no. 4, pp. 1808–1816, 2017, doi: 10.1007/s11665-017-2627-5.

[30] B.Q. Han, K.C. Chan, T.M. Yue, and W.S. Lau, "High temperature deformation behavior of Al 2124-SiC_p composite," *J. Mater. Process. Tech.*, vol. 63, no. 1–3, pp. 395–398, 1997, doi: 10.1016/S0924-0136(96)02653-2.

[31] P. Yu *et al.*, "Interfacial reaction during the fabrication of $Ni_{60}Nb_{40}$ metallic glass particles-reinforced Al based MMCs," *Mater. Sci. Eng. A*, vol. 444, no. 1–2, pp. 206–213, 2007, doi: 10.1016/j.msea.2006.08.077.

[32] Y.K. Xu, M. Han, X. Jian, and E. Ma, "Mg-based bulk metallic glass composites with plasticity and gigapascal strength," *Acta Mater.*, vol. 53, no. 6, pp. 1857–1866, 2005, doi: 10.1016/j.actamat.2004.12.036.

[33] J. Fan, K. Zhnag, and L. Shi, "Interface Characterization of the SiCp/Al Composites Made by Powder Metallurgy," *J. Mater. Sci. Technol.*, vol. 15, no. 2, pp. 147–150, 1999, https://www.jmst.org/EN/abstract/abstract5749.shtml.

[34] J.-Ch., Lee, and, J.-Y. Byun, S.-B. Park, and H.-I. Lee, "Prediction of Si contents to suppress the formation of Al_4C_3 in the SiCp/Al composite," *Acta Mater.*, vol. 46, pp. 1771–1780, 1998, doi: 10.1016/S1359-6454(97)00265-6.

[35] J.K. Park and J.P. Lucas, "Moisture effect on SiC_p/6061 Al MMC: Dissolution of interfacial Al_4C_3," *Scripta Mater.*, vol. 37, no. 4, pp. 511–516, 1997, doi: 10.1016/S1359-6462(97)00133-4.

[36] J. Long-tao *et al.*, "Microstructure and tensile properties of TiB_{2p}/6061Al composites," *Trans. Nonferrous Met. Soc. China*, vol. 19, no. 8, pp. 542–546, 2009, doi: 10.1016/S1003-6326(10)60105-7.

[37] B. Ogel and R. Gurbuz, "Microstructural characterization and tensile properties of hot pressed Al–SiC composites prepared from pure Al and Cu powders," *Mater. Sci. Eng. A*, vol. 301, no. 2, pp. 213–220, 2001, doi: 10.1016/S0921-5093(00)01656-7.

[38] Y. Qiao *et al.*, "Effect of hydrogen charging on microstructural evolution and corrosion behavior of Ti-4Al-2V-1Mo-1Fe alloy," *J. Mater. Sci. Technol.*, vol. 60, pp. 168–176, 2021, doi: 10.1016/j.jmst.2020.06.010.

[39] Y.X. Qiao *et al.*, "Corrosion Behavior of a Nickel-Free High-Nitrogen Stainless Steel With Hydrogen Charging," *JOM*, vol. 73, no. 4, pp. 1165–1172, 2021, doi: 10.1007/s11837-021-04569-2.

[40] J. Wu, Y. Qiao, Y. Chen, L. Yang, X. Cao, and S. Jin, "Correlation between Corrosion Films and Corrosion-Related Defects Formed on 316 Stainless Steel at High Temperatures in Pressurized Water," *J. Mater. Eng. Perform.*, vol. 30, pp. 3577–3585, 2021, doi: 10.1007/s11665-021-05688-2.

[41] S. Lesz, B. Hrapkowicz, K. Gołombek, M. Karolus, and P. Janiak, "Synthesis of Mg-based alloys with a rare-earth element addition by mechanical alloying," *Bull. Pol. Acad. Sci. Tech. Sci.*, vol. 69, no. 1, p. e137586, 2021, doi: 10.24425/bpasts.2021.137586.